Int. J. Multiphase Flow Vol. 16, No. 1, pp. 43–56, 1990
Printed in Great Britain. All rights reserved

0301-9322/90 $3.00 + 0.00
Copyright © 1990 Pergamon Press/Elsevier

PARTICLE DIFFUSIVITY IN FULLY DEVELOPED, TURBULENT, HORIZONTAL PIPE FLOW OF DILUTE AIR–SOLID SUSPENSIONS

S. NI
H. A. Phillips & Co., St Charles, IL 60174, U.S.A.

B. T. CHAO† and S. L. SOO
Department of Mechanical and Industrial Engineering, University of Illinois at Urbana-Champaign, Urbana, IL 61801, U.S.A.

(*Received* 19 *October* 1988; *in revised form* 1 *June* 1989)

Abstract—The diffusivity of small particles in steady, horizontal pipe flows of dilute air–solid suspensions under the influence of gravity and weak electrostatic forces was studied. An isokinetic sampling system, a density probe with randomized bifurcated fiber optics and a Faraday cage were used to measure distributions over a cross section of particle mass flux, particle phase density and the locally averaged particle charge-to-mass ratio. The local particle diffusivity was then determined by using the mass and charge conservation equations. For alumina particles of equivalent volume diameter of 31 μm, pipe Reynolds number of 7.21×10^4, 1.41×10^5 and 2.15×10^5, a solid-to-air mass ratio up to 0.4 and a particle charge-to-mass ratio up to 1.6×10^{-4} C/kg, the fluid–solid interaction is the dominating mechanism that controls particle diffusivity. The gravitational and electrical forces have only a very minor influence.The data reveal that the particle diffusivity is not uniformly distributed over the pipe cross section, contrary to the assumption of uniform diffusivity commonly used in the literature. However, it was found that the product of particle diffusivity and inverse relaxation time is almost a constant over the cross section. A simple formula for the approximate evaluation of the constant is given.

Key Words: particle diffusivity, fully developed, turbulent, horizontal pipe flow, air–solid

1. INTRODUCTION

The transport behavior of small particles in a turbulent flowfield under the influence of gravitational and electrostatic field forces is of prime interest to meteorologists and chemical, civil, environmental, mechanical and nuclear engineers. Since the late 1940s, a great deal of effort has been expended to describe the dynamic behavior of a small spherical particle suspended in stationary, homogeneous, turbulent flows by the Lagrangian equation of motion (Tchen 1947; Soo 1956; Lumley 1957; Chao 1964; Meek & Jones 1973 etc.). Rigorous solutions are difficult because of the statistical nonlinearity arising from the random nature of turbulent flow and the fact that the particle does not generally follow the fluid motion. Some sort of empiricism is often introduced for practical applications. A well-known example is Csanady's (1963) treatment of the cross-trajectory effect. Attempts to extend the analysis to clouds of suspended particles were hindered by the additional complexity of the mutual interactions between the particle and the fluid and among the particles. A convenient and useful approach is to express the turbulent transport of mass or momentum as the product of a transport coefficient and the spatial gradient of the appropriate mean variable. One such coefficient is the particle diffusivity. Unlike the molecular diffusivity of a fluid, it is not a true material property. While the limitations of the concept of particle diffusivity are well-known, it is nevertheless useful and has been widely adopted in engineering practices. It is an important parameter in the scaling and modeling of suspension flows (Chao 1981). Unfortunately, there is a dearth of experimental data on particle diffusivity, and its assessment even for the simple case of fully developed pipe flow of dilute suspensions cannot be readily made. A review of the subject can be found in a paper by Soo (1978).

In this paper, results are presented for the radial and azimuthal distributions of particle diffusivity in fully developed, turbulent, horizontal pipe flows of dilute air–solid suspensions. The

†To whom all correspondence should be addressed.

particles were either naturally charged by contact or weakly charged by a corona charger in air of controlled relative humidity. Within the range of the experimental variables used in the study, it was found that the local particle diffusivity can be correlated with the local eddy diffusivity of the carrier fluid and the inverse relaxation time for particle–fluid interactions. The gravitational and electrostatic forces have a weak influence on particle diffusivity when the Froude number and the pipe Reynolds number are sufficiently large.

2. METHOD OF DETERMINATION OF PARTICLE DIFFUSIVITY

2.1. Assumptions and basic equations

In the present study, the distribution of particle diffusivity in the vertical cross section of a horizontal, steady, fully developed pipe flow of dilute air–solid suspensions was evaluated from measured local particle mass flux, local particle phase density and local electrostatic charge-to-mass ratio of particles with the aid of mass and charge conservation equations. These conservation equations have been given by Soo (1973). The major assumptions are:

1. The suspension is dilute and consists of monodispersed spheres.
2. The system is isothermal and the gaseous phase is incompressible.

For the system under study, the momentum equation for the particulate phase is

$$F(\mathbf{U}-\mathbf{U}_p)+\mathbf{f}+\frac{1}{\rho_p}\nabla\cdot\tau_p=0, \qquad [1]$$

where F is the inverse relaxation time for particle–fluid interactions, $\mathbf{U}$ and $\mathbf{U}_p$ denote, respectively, the fluid and particle velocity vector, ρ_p is the density of the particulate phase and τ_p is its stress tensor. The field force $\mathbf{f}$ has two distinct origins: (a) gravity and (b) electrostatic force due to the particles' electric change. It is given by

$$\mathbf{f}=\boldsymbol{g}\left(1-\frac{\bar{\rho}}{\bar{\rho}_p}\right)+\frac{q}{m_p}\nabla V_e, \qquad [2]$$

where $\boldsymbol{g}$ is the gravitational acceleration, $\bar{\rho}$ and $\bar{\rho}_p$ are the material densities of the fluid and the particle, respectively, q is the average charge carried by a particle, m_p is the particle mass and V_e is the electric potential. q/m_p is commonly known as the charge-to-mass ratio. For the current system, the field force $\mathbf{f}$ gives rise to drift fluxes in the plane perpendicular to the horizontal pipe axis. In this plane, τ_p is negligible and the momentum equation simplifies to

$$F(\mathbf{U}_p-\mathbf{U})_\perp=\mathbf{f}=\boldsymbol{g}\left(1-\frac{\bar{\rho}}{\bar{\rho}_p}\right)+\frac{q}{m_p}\nabla V_e, \qquad [3]$$

where the subscript $\perp$ refers to the plane perpendicular to the pipe axis. By definition, fully developed flow requires that all derivatives with respect to the axial direction vanish and, hence, possible deposition and reentrainment of the particles are not considered. Consequently, the mass flux due to relaxation under the field force, $\rho_p(\mathbf{U}_p-\mathbf{U})_\perp$, must be balanced by the mass flux due to diffusion, $-D_p\nabla\rho_p$, where D_p is the turbulent mass diffusivity of the particulate phase, assumed to be a scalar. Accordingly,

$$D_p\nabla\rho_p+\frac{\rho_p}{F}\frac{q}{m_p}\nabla V_e+\frac{\rho_p}{F}\boldsymbol{g}\left(1-\frac{\bar{\rho}}{\bar{\rho}_p}\right)=0. \qquad [4]$$

If r and ϕ denote, respectively, the radial and azimuthal coordinates of a cylindrical coordinate system with $\phi=0$ coinciding with the top of the pipe, then

$$D_p\frac{\partial\rho_p}{\partial r}+\frac{\rho_p}{F}\frac{q}{m_p}\frac{\partial V_e}{\partial r}+\frac{\rho_p}{F}\left(1-\frac{\bar{\rho}}{\bar{\rho}_p}\right)g\cos\phi=0 \qquad [4a]$$

and

$$\frac{D_p}{r}\frac{\partial\rho_p}{\partial\phi}+\frac{\rho_p}{F}\frac{q}{m_p}\frac{1}{r}\frac{\partial V_e}{\partial\phi}-\frac{\rho_p}{F}\left(1-\frac{\bar{\rho}}{\bar{\rho}_p}\right)g\sin\phi=0. \qquad [4b]$$

While, in principle, either [4a] or [4b] may be used for the evaluation of D_p; in practice, [4a] is preferred for two reasons. First, as we shall soon demonstrate, $\partial V_e/\partial r$ along the vertical diameter can be determined from an integral and hence with greatly improved accuracy. Second, it is experimentally more convenient to measure ρ_p and q/m_p along the radial direction than along the azimuthal direction. The inverse relaxation time F is given by (Soo 1973):

$$F = m_p \frac{\text{drag}}{|\mathbf{U} - \mathbf{U}_p|} = C^* F_S \left(1 + \frac{\bar{\rho}}{2\bar{\rho}_p}\right)^{-1}, \qquad [5]$$

where F_S denotes the inverse relaxation time for Stokes motion. For a spherical particle of radius a, $F_S = 9\mu/2a^2\bar{\rho}_p$, μ being the dynamic viscosity of the fluid. In [5], C^* is a correction factor to account for the deviation from the Stokesian drag:

$$C^* = \frac{C_D}{24} \mathrm{Re}_p, \qquad [6]$$

in which C_D is the drag coefficient and Re_p is the particle Reynolds number based on the relative motion, defined by

$$\mathrm{Re}_p = \frac{2a|\mathbf{U} - \mathbf{U}_p|}{\nu} \simeq \frac{2a|W - W_p|}{\nu}, \qquad [7]$$

where ν is the kinematic viscosity of the fluid and W and W_p are the temporal mean of the axial velocity components of the fluid and the particle, respectively. The approximation involved in replacing $|\mathbf{U} - \mathbf{U}_p|$ by $|W - W_p|$ is acceptable since the flow is predominantly axial and the fluid and particle turbulence usually amounts to a few percent of their respective temporal means. In a dilute suspension, W can be assumed to be undisturbed by the presence of the particles, and hence the power law is applicable. Indeed, this has been found to the case in the present study (Ni 1986). Denoting the centerline velocity by W_0, and the inner pipe radius by R, we have

$$W = W_0 \left(1 - \frac{r}{R}\right)^n. \qquad [8]$$

In the present investigation, the measured data fit [8] very well by assigning $n = 1/7$. An empirical equation for C_D, proposed by Soo (1983), is

$$C_D = \left(\frac{24}{\mathrm{Re}_p}\right)(1 + 0.00975\,\mathrm{Re}_p - 0.636 \times 10^{-3}\,\mathrm{Re}_p^2), \qquad [9]$$

for $\mathrm{Re}_p < 100$. The alumina particles used in this study have a material density $\bar{\rho}_p = 3800\ \mathrm{kg/m^3}$. The carrier air was essentially at room temperature and pressure, giving $\bar{\rho} = 1.21\ \mathrm{kg/m^3}$. Thus, $\bar{\rho}/\bar{\rho}_p = 3.2 \times 10^{-4}$ and $(1 - \rho/\rho_p)$ in [4a] or [4b] and $(1 + \bar{\rho}/2\bar{\rho}_p)$ in [5] can be replaced by unity.

Accordingly, the mass conservation equation used is

$$D_p \frac{\partial \rho_p}{\partial r} + \frac{\rho_p}{F} \frac{q}{m_p} \frac{\partial V_e}{\partial r} + \frac{\rho_p}{F} g \cos\phi = 0. \qquad [10]$$

The charge conservation equation is the well-known Poisson equation:

$$\frac{1}{r}\frac{\partial}{\partial r}\left(r \frac{\partial V_e}{\partial r}\right) + \frac{1}{r^2}\frac{\partial^2 V_e}{\partial \phi^2} = -\frac{1}{\epsilon_0}\rho_p \frac{q}{m_p}, \qquad [11]$$

with the boundary condition

$$V_e = 0 \qquad \text{at } r = R \text{ (grounded pipe wall)} \qquad [11a]$$

and the symmetry condition along the vertical diameter

$$\frac{\partial V_e}{\partial \phi} = 0, \qquad \text{for } \phi = 0 \text{ and } \pi. \qquad [11b]$$

In addition, V_e must be finite at $r = 0$. In [11], ϵ_0 is the electric permittivity in a vacuum ($= 1/36\pi \times 10^{-9}\ \mathrm{F/m}$). The scheme used for evaluating the local particle diffusivity D_p is illustrated in figure 1. Using the measured ρ_p and q/m_p, V_e was calculated from [11] with a finite-difference

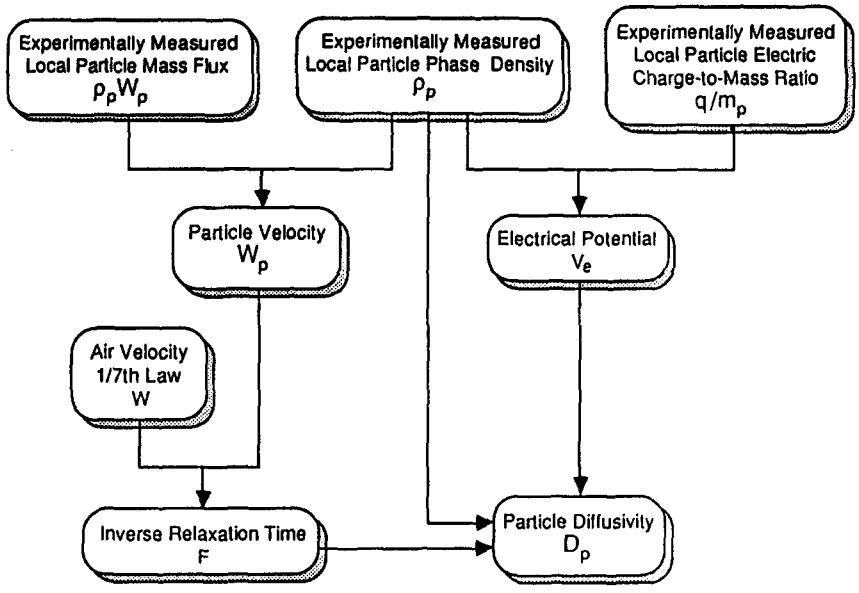

Figure 1. Scheme for evaluation of local particle diffusivity from measured mass flux, density and charge-to-mass ratio.

scheme. The local particle velocity W_p was obtained by dividing the measured local particle mass flux by ρ_p. Hence $(W - W_p)$ became known, and Re_p could then be calculated from [7] and C_D from [9]. The inverse relaxation time F was then obtained from [5] with $(1 + \bar{\rho}/2\bar{\rho}_p)^{-1}$ replaced by unity. With the availability of ρ_p, q/m_p, V_e and F, [10] becomes an algebraic equation for D_p.

Along the vertical diameter, $\partial V_e/\partial\phi = 0$, and, in addition, the study by Nieh *et al.* (1985a) showed that $r^{-2}\,\partial^2 V_e/\partial\phi^2 \ll r^{-1}\,\partial/\partial r(r\,\partial V_e/\partial r)$, hence [11] can be integrated to give

$$\frac{\partial V_e}{\partial r} = -\frac{1}{\epsilon_0}\frac{1}{r}\int_0^r \rho_p \frac{q}{m_p} r\,\mathrm{d}r. \qquad [12]$$

Thus, the use of numerical differentiation for evaluating $\partial V_e/\partial r$ is avoided.

2.2. *Modifications for nonspherical particles*

The stock of alumina particles supplied by the manufacturer was sieved three times with U.S. standard sieve Nos 325 and 270, corresponding to mesh sizes of 45 and 55 μm. Photographs of the sieved particles taken with a microscope revealed that they were irregularly shaped. In the literature several equivalent diameters have been used to characterize irregularly shaped particles. They are the Martin's diameter d_M, Feret's diameter d_F, the projected area diameter d_{pa} and the equivalent volume diameter d_e (Hinds 1982). The frequency distributions of d_M and d_F of the alumina particles were determined and their mean values were found to be 39 and 48 μm, respectively. In general, $d_M \leqslant d_{pa} \leqslant d_F$ and the equality holds for spheres. For irregularly shaped particles associated with crushed minerals, d_M is only slightly less than d_{pa}, and they are often taken to be equal. Since d_e is defined as the diameter of the sphere having the same volume as the irregular particle, the particle mass m_p is $(\pi/6)d_e^3\bar{\rho}_p$. A volume shape factor α_v has been used by Hinds to relate d_{pa} and d_e. The relation is $(\pi/6)d_e^3 = \alpha_v d_{pa}^3 \simeq \alpha_v d_M^3$.

The drag force acting on a particle translating in a fluid also depends on its shape. A dynamic shape factor χ (Hinds 1982) has been used to account for such an effect. It is defined as the ratio of the actual resistance force of the nonspherical particle to that of a sphere having the same volume and velocity. Accordingly, one modifies [5] to read

$$F = \chi C^* F_s \qquad [13]$$

when $\bar{\rho}/\bar{\rho}_p \ll 1$. While an accurate determination of α_v and χ is difficult, an estimate can be made for the alumina particles. Hinds' book lists the values of both factors for a number of crushed minerals, including sand, glass, china clay, quartz, limestone etc. The variations in both α_v and χ

are $< 20\%$. Since the mechanical properties of sand and alumina are similar, the two shape factors for sand recommended by Hinds, namely, $\alpha_v = 0.26$ and $\chi = 1.57$, were used for alumina. Accordingly, $d_e/d_M = (6 \times 0.26/\pi)^{1/3} = 0.792$, giving $d_e = 31\ \mu m$.

3. EXPERIMENTAL FACILITIES AND INSTRUMENTATION

3.1. Continuous flow test loop with cyclone separator and venturi feeder

A continuous flow test loop for an air–solid suspension with a cyclone–venturi configuration for the separation and reintroduction of particles is shown in figure 2. A Buffalo Type 45-1 high pressure blower with a variable-speed motor drive produces average air velocities up to 41 m/s in the 127 mm dia copper pipe loop. The solid particles collected in the cyclone separator are reintroduced into the flow stream at the throat of the venturi feeder (14). The suspension flows through a corona charger (10) and becomes fully developed in the test section. A portion of the test section (7) is equipped with quartz windows for visual observation. The suspension then enters a transition piece (6) which connects the circular exit of the test section to the rectangular entrance of a cyclone separator. A vortex regulating valve (5) controls the angular momentum of the suspensions entering the cyclone separator to provide the desired pressure level for the free flow of particles, a high collection efficiency and at the same time to minimize breakage as the particles enter the cyclone. The clean air flows into a plenum chamber (3) where it is cooled by a heat exchanger and then reenters the blower. In this way, attrition or breakage of particles due to impaction on the blower blades is avoided. The rotatable section (15) was used for probes to traverse along a diameter inclined at any angle from the vertical. Details of the flow loop, the cyclone separator and the venturi feeder can be found in the thesis by Ni (1986).

The local particle mass flux was measured by an isokinetic sampler. Its theory, operations procedure and error source have been discussed by Soo *et al.* (1969). Ni (1986) described an improved design that made possible the quick establishment of the local isokinetic condition.

3.2. Particle phase density measurement

The density distribution of the particulate phase was measured by an optical density probe, shown in figure 3. It is an improved version of the earlier probe used by Soo *et al.* (1964). Randomized bifurcated fiber optics are used to transmit both the source light and the signal light in the same cable. Light originating from the illuminator (1) enters the fiber optics cable (2-1). One arm of the cable (2-2) is connected to arm 3-2 of another randomized bifurcated cable 3-1. The light passing through arm 3-2 and cable 3-1 enters the glass tube 4, scattered by the suspended

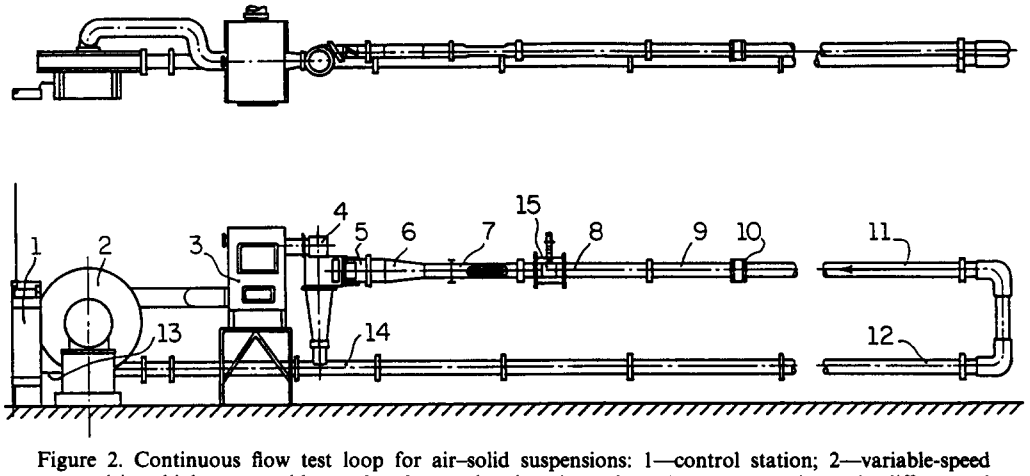

Figure 2. Continuous flow test loop for air–solid suspensions: 1—control station; 2—variable-speed motor-driven high-pressure blower; 3—plenum chamber; 4—cyclone; 5—vortex regulator; 6—diffuser and transfer piece; 7—test section with optical windows; 8—test section No. 1; 9—test section No. 2; 10—corona charger; 11—pipe; 12—pipe; 13—power cable; 14—injection venturi; 15—rotatable test section.

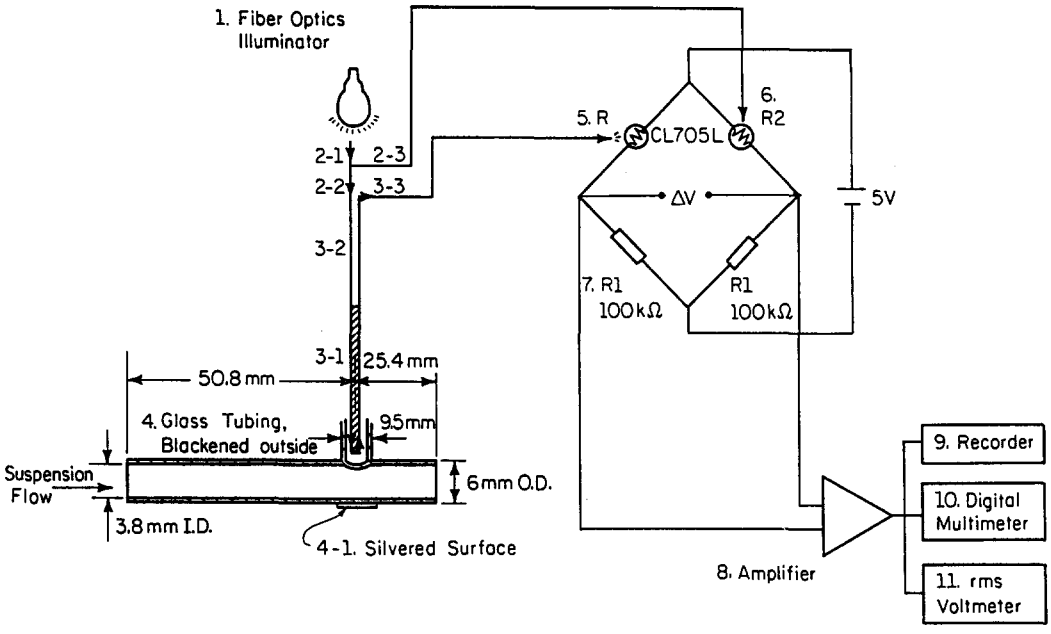

Figure 3. Optical density probe system.

particles, and is then reflected by the silvered surface 4-1. The glass probe 4 is blackened externally and is of sufficient length to shield the stray light reflected from the highly glossy interior surface of the pipe wall. The reflected light from the silvered surface passes through cables 3-1 and 3-3, and finally reaches a Clairex photocell (5). The second path of light from source 1 passes through cables 2-1 and 2-3 and reaches another photocell (6) which is identical to 5. The use of photocells 5 and 6 in a bridge circuit eliminates the deleterious effect of the fluctuations of light source 1 on the bridge output voltage ΔV. The bridge output is amplified by a high gain, low noise d.c. bridge preamplifier and then displayed on a recorder, an r.m.s. voltmeter and a digital multimeter. The disturbance due to the presence of the probe on the trajectory of the solid particles has been found negligible because of the particle inertia.

Using Bouguer's law for the attenuation of monochromatic radiation passing through a scattering–absorbing medium together with bridge circuit algebra, Ni (1986) obtained

$$\Delta\rho_p = K^*\Delta V, \qquad [14]$$

where ΔV is the change in bridge output and $\Delta\rho_p$ is the corresponding change in particle phase density. The probe constant K* was determined by calibration. The particle velocity at the pipe centerline was measured by an electrostatic induction probe (Nieh *et al.* 1986). The average velocity lag at the centerline was found to be 3.5% for the range of air velocities investigated. Using the measured particle mass flux, the particle density is obtained. Hence, by determining the change in particle phase density and the corresponding change in the bridge output at several centerline air velocities, the probe constant K* can be evaluated and its average was found to be 134.7 kg/m^3 V. The reliability of the density measurement was maintained by frequent calibration.

3.3. Control of the particle charge-to-mass ratio and its measurement

Turner & Blasubramanian (1976) and Nieh *et al.* (1985b) reported that relative humidity had a significant influence on the average charge and charge distribution of particles in air–solid flows. This observed phenomenon was utilized in the present study to control, in part, the particle charge-to-mass ratio. Since the relative humidity of the carrier air depends on its temperature, an automobile radiator was installed in the plenum chamber (3 in figure 2) for this purpose. A three-row, four-column corona charger was fabricated for enhancing, neutralizing and reversing the charge carried by the particles. Since the alumina particles used in the study were positively charged by contact with the walls of the copper pipe, positive corona was used for raising the

charge-to-mass ratio. On the other hand, negative corona was used for neutralizing and reversing the charges.

A Faraday cage in conjunction with a sampling probe, a charge-to-voltage converter, a Royco counter and the associated signal processing system were used for the charge spectrum measurements. Mean values of q/m_p evaluated from the spectral data compare favorably with those determined from electric current measurements. Details have been given by Ni (1986).

4. EXPERIMENTAL RESULTS AND DISCUSSIONS

Sieved alumina particles of $\bar{\rho}_p = 3800\ \text{kg/m}^3$ and $d_e = 31\ \mu\text{m}$ and room air flowing in a 127 mm copper pipe at pipe Reynolds numbers of $\text{Re} = 7.21 \times 10^4$, 1.41×10^5 and 2.15×10^5 ($\text{Re} = 2RW_{av}/\nu$, where W_{av} is the area-averaged velocity), were used in the experimentation. The corresponding centerline velocities were 10.6, 20.7 and 31.6 m/s. The dilute suspension flow reached the test section after passing through a length of approx. 60 dia downstream of the last 90° bend, thus the air flow could be taken to be fully developed. To ascertain if the particle flow was also fully developed, the distributions of particle mass flux and the mean charge-to-mass ratio along a vertical diameter were measured both at the test section and at the location 0.66 m further downstream for each of the three velocities used. The differences were found to be insignificant, assuring that the suspension flow was indeed fully developed.

4.1. Gravitational effects on the dynamics of particle suspension and particle diffusivity

Measured particle phase density distributions along diameters in a vertical plane with $\phi = 0°$, 30°, 60° and 84° are shown in figure 4 for centerline velocity $W_0 = 31.6$ m/s, and the corresponding $\text{Re} = 2.15 \times 10^5$. All densities are normalized by the centerline value $\rho_{po} = 0.137\ \text{kg/m}^3$. The data for $\phi = 0°$ are for the vertical diameter and $\phi = 84°$ are for the near-horizontal direction. Along the horizontal diameter, $\partial\rho_p/\partial r = 0$, and hence the particle diffusivity D_p cannot be evaluated from [10]. Since the density, mass flux and charge distributions were all symmetrical with respect to the vertical diameter, measurements were conducted only in the first and third quadrants of the cross section. In this series of experiments, the corona charger was not activated and the charging of particles was due to natural contact. At the pipe centerline, the mean charge-to-mass ratio, $(q/m_p)_0$, was 2.36×10^{-6} C/kg which was very low. By numerically integrating the measured density over the cross section, the mass loading of the suspension flow can be calculated. In the present case, the solid-to-air mass loading was 0.2 and the average particle phase density was 0.25 kg/m^3. Along the vertical diameter, there is almost a 5-fold increase from the top to the bottom of the pipe due to the influence of gravity. As ϕ increases, the gravitational effect decreases as expected. However, at $\phi = 84°$, the gravitational effect can still be discerned.

Figure 5 presents the particle mass flux distributions. All values are normalized by the centerline flux $G_0 = 4.18\ \text{kg/m}^2\,\text{s}$. The effect of gravity is again clearly revealed. Along the vertical diameter, the particle mass flux increases monotonously from the top downward, until the region near the

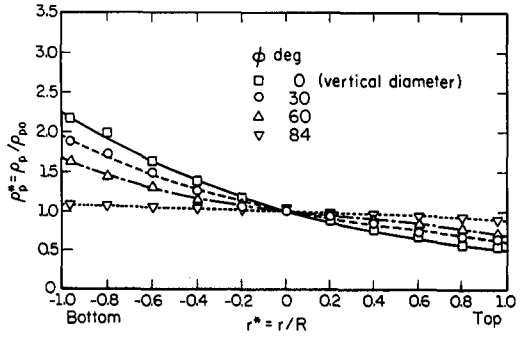

Figure 4. Particle density distribution in a vertical cross section. Centerline air velocity, $W_0 = 31.6$ m/s; centerline particle density, $\rho_{p0} = 0.137\ \text{kg/m}^3$.

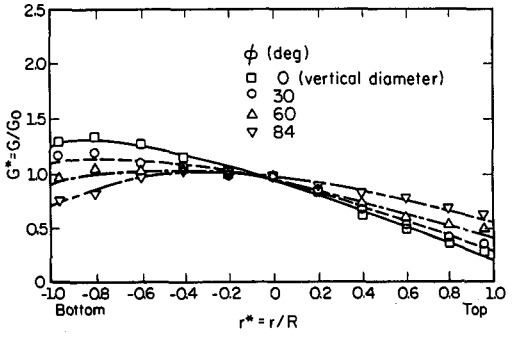

Figure 5. Particle mass flux distribution in a vertical cross section. Centerline air velocity, $W_0 = 31.6$ m/s; centerline particle mass flux, $G_0 = 4.18\ \text{kg/m}^2\,\text{s}$.

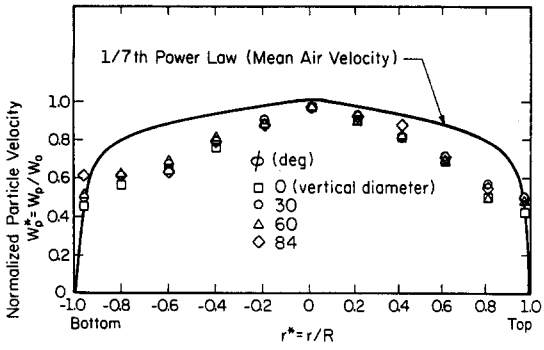

Figure 6. Particle axial velocity distribution in a vertical cross section. Centerline air velocity, $W_0 = 31.6$ m/s; centerline particle charge-to-mass ratio, $(q/m_p)_0 = 2.36 \times 10^{-6}$ C/kg).

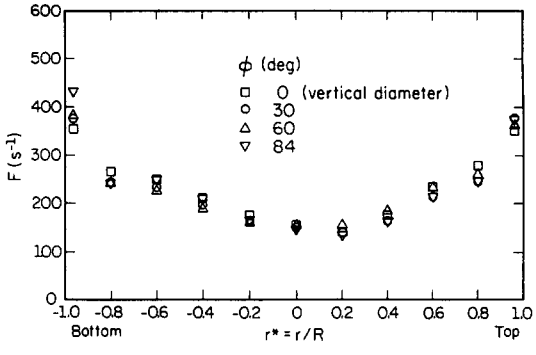

Figure 7. Distribution of the inverse relaxation time of particles in a vertical cross section. Centerline particle mass flux, $G_0 = 4.18$ kg/m^2 s; pipe Re $= 2.15 \times 10^5$.

bottom of the pipe is reached ($r^* \simeq -0.8$) where it attains a maximum, beyond which the particle mass flux decreases as a result of the reduction in particle velocity. As ϕ increases, the asymmetry of the particle mass flux distribution relative to the pipe center becomes less pronounced. It becomes nearly symmetric for $\phi = 84°$.

The mean axial velocity distributions of the particles are shown in figure 6. All data are normalized by W_0. As pointed out earlier, the measured air velocities appeared to be relatively unaffected by the presence of the particles and could be well-represented by the 1/7th power law.† It is seen that the particle mean axial velocity profiles are very nearly symmetrical with respect to the center of the cross section for all azimuthal angles, despite the large differences in the particle phase density. This suggests that the influence of gravity on the particle mean axial velocity in dilute suspensions is insignificant, as expected. The same can be said for the inverse relaxation time for particle–fluid interactions, shown in figure 7. The inverse relaxation time reaches its local minimum value at the pipe center where the velocity lag between particles and the fluid is relatively small. It increases towards the wall as the velocity lag increases. In the region near the wall, while the air velocity decreases rapidly towards zero as the wall is approached, the particle velocity decreases much more slowly and reaches a finite value (relative velocity) at the wall. Thus, there exists a location near the wall where the relative velocity of the particle to the fluid vanishes and the inverse relaxation time reaches the theoretical minimum of $9\mu/2a^2\bar{\rho}_p$. However, this is not revealed by the data shown in figure 7. We shall return to this point later.

Using the procedure illustrated in figure 1, the local particle diffusivity was evaluated and the results are presented in figure 8. The distribution of particle diffusivity along the near-horizontal diameter ($\phi = 84°$) is very nearly symmetric with respect to the pipe center. It peaks at the center and gradually decreases towards the wall. Along the vertical diameter, the distribution is skewed, with generally smaller values of D_p in the lower half of the cross section. This can be attributed to the higher particle concentration, which results in the greater mechanical energy dissipation of the carrier air and hence lowers the turbulent diffusivity of both the air and the particles.

4.2. Effects of the interaction of gravity and pipe Reynolds number on the dynamics of the particle suspension and particle diffusivity

To examine the combined influence of gravity and fluid turbulence on the dynamics of the particle suspension, measurements of particle phase density and mass flux distributions were made along the vertical diameter of the test section for the three pipe Reynolds numbers. The solid–air mass loading was the same as before. While there were variations in the particle charge, $(q/m_p)_0$ was very small for all cases, being of the order of 10^{-6} C/kg. Figure 9 shows the particle phase

†It should be noted that this might not be true when the particle diameter is large, the pipe flow Reynolds number is not sufficiently high and the solid-to-air mass ratio is large. Tsuji & Morikawa (1982) reported that plastic particles of 0.2 and 3.4 mm dia transported at average air velocity of 6–20 m/s in a 30 mm pipe produced a significant effect on the air velocity profile, particularly when the mass loading was high.

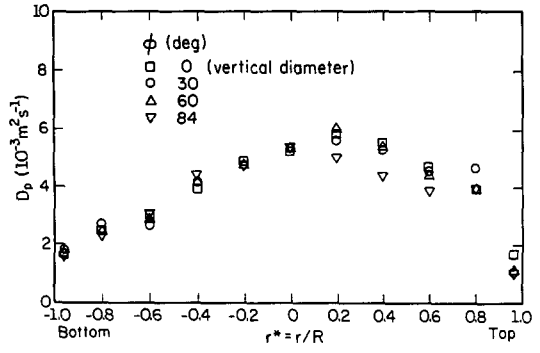

Figure 8. Distribution of particle diffusivity in a vertical cross section. Centerline air velocity, $W_0 = 31.6$ m/s; centerline particle mass flux, $G_0 = 4.18$ kg/m^2 s; pipe Re = 2.15×10^5.

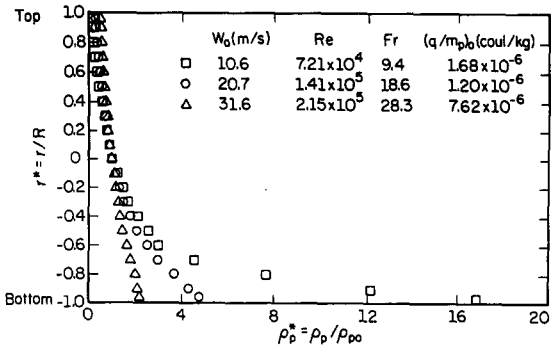

Figure 9. Influence of pipe Re on the particle density distribution along a vertical diameter.

density distributions along the vertical diameter. To compare the gravitational influence at different air velocities, we introduce the Froude number, defined by

$$\mathrm{Fr} = \frac{W_0}{(2\,Rg)^{1/2}}. \qquad [15]$$

The nonuniformity in the particle density distribution is seen to increase rapidly as Fr decreases, indicating the increasingly dominating influence of gravity over that of turbulent diffusion. At Fr = 9.4, the particle phase density at the bottom of the pipe was about 200 times that at the top. The locally high particle concentration would retard the local air velocity. A similar phenomenon is also seen in figure 10 for the particle mass flux distribution. The particle mass flux increases from the top of the pipe downward along the vertical diameter and reaches a maximum value in the region near the bottom wall. It then decreases due to the greater decrease in particle velocity than the increase in particle phase density.

Figure 11 illustrates the particle mean axial velocity distributions for the three pipe Re values. All particle velocities are also normalized by W_0. It is seen that the particle velocity profiles resemble that for laminar flow, particularly when Re is high. At a given radial location, the particle mean velocity normalized by the air centerline velocity decreases slightly and the normalized velocity lag of the particle increases slightly as Re increases. This finding is in agreement with measurements in pulverized coal made by Cheng *et al.* (1970).

For alumina particles of $\chi = 1.57$, $F_S = 118$ s^{-1}, and F can be evaluated from [13]. Values of Re_p at the pipe center corresponding to $\mathrm{Re} = 7.21 \times 10^4$, 1.41×10^5 and 2.15×10^5 are 0.37, 0.73 and 1.12, respectively. The corresponding values of F at the pipe centerline are 122.1, 126.4 and 130.9 s^{-1}. Figure 12 shows the distributions of F along the vertical diameter for the three Re values just cited. Since the velocity lag between the fluid and the particle increases with air velocity, F generally increases with Re, as exhibited in the figure. For a given Re, F attains a local minimum at the pipe center due to the small velocity lag. As one moves radially away from the center, F increases first, attains a maximum and then decreases with further increases in r due to the reduction in velocity lag as the wall is approached. As pointed out in section 4.1, there exists a location where the velocity lag vanishes. At this location, F assumes its theoretical minimum value although it is next to impossible to detect it experimentally due to the steep gradients of both air and solid velocities. As one moves further towards the wall, the velocity lag again increases, resulting in larger values of F, as exhibited in figure 12 for all three pipe Re.

The influence of pipe Reynolds number on particle diffusivity is shown in figure 13. The turbulence intensity of the air flow increases with Re and so does the particle diffusivity. The error flags shown were based on a detailed assessment by Ni (1986) of the various error sources. When D_p is normalized by u^*R, with $u^* = W_{av}(f/8)^{1/2}$, f being the friction factor, all data can be collapsed to lie within a narrow band, as shown in figure 14. The relatively large scatter for $\mathrm{Re} = 7.21 \times 10^4$ is, at least in part, due to the measurement error associated with the isokinetic sampling system at low velocities. Included in the figure is the distribution of air eddy diffusivity for momentum

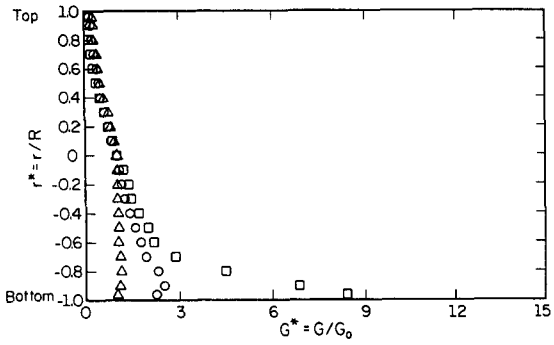

Figure 10. Influence of pipe Re on the particle mass flux distribution along a vertical diameter. Key as in figure 9.

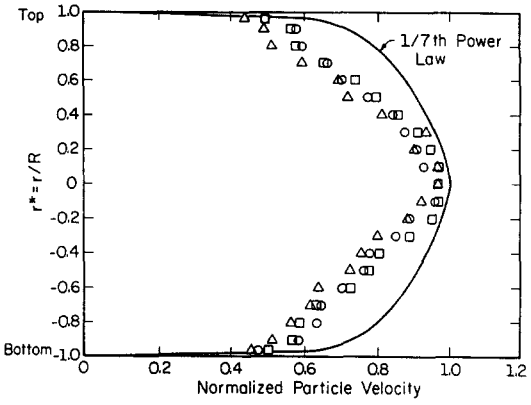

Figure 11. Influence of pipe Re on the particle axial velocity distribution along a vertical diameter. Key as as in figure 9.

transfer ϵ_m in fully developed pipe flow at moderately large Reynolds numbers. The data were taken from Hinze (1975). In the wall region, ϵ_m was evaluated from the measured shear stress and the mean velocity distributions in air flow reported by Laufer (1954) and by Nunner (1956). Seamless smooth tubes were used in Laufer's experiments but rough pipes were used by Nunner. The air eddy diffusivity first increases almost linearly with distance from the wall (except for the region very close to the wall), reaches a maximum at $r^* \simeq \pm 0.7$, then decreases slightly and attains a nearly constant value in the core region. At $r^* = 0$, ϵ_m cannot be evaluated since the mean velocity profile is axisymmetric. However, in the core region, the turbulence is nearly isotropic, and the eddy diffusivity may be assumed to be constant—as illustrated by the dashed line in the figure. Very close to the wall ($r^* \simeq \pm 1$), R is not the appropriate length scale and hence the curve is again shown by dashed lines. While the fluid diffusivity is expected to be axisymmetrical, the particle diffusivity is not, particularly for the smallest pipe Re tested. This can be attributed to the influence of gravity on the density distribution along the vertical diameter. The particle diffusivity shows a peak in the core region of the pipe, slightly above the centerline. Particles in this region have a relatively small velocity lag behind the air. This, coupled with the fact that the eddies are relatively large in this region, tends to minimize the cross-trajectory effect, resulting in higher values of particle diffusivity. In the wall region, the particle diffusivity exhibits a small rise due to the increasing turbulent intensity of the air flow. It then decreases rapidly in the region very near the wall because of the suppression of fluid turbulence as the wall is reached. At certain locations near the wall, the particle diffusivity exceeds that of the air. This is plausible since the air velocity must necessarily vanish at the wall while the particle will, in general, have a finite sliding velocity.

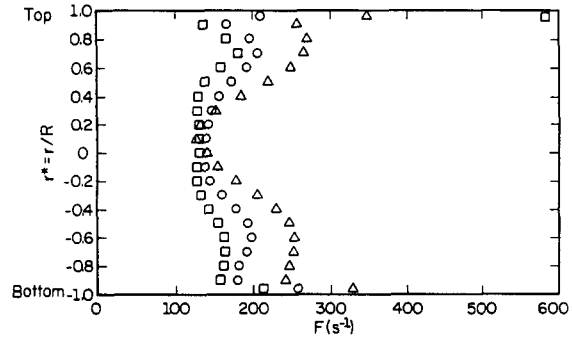

Figure 12. Influence of pipe Re on the distribution of the inverse relaxation time of particles along a vertical diameter. Key as in figure 9.

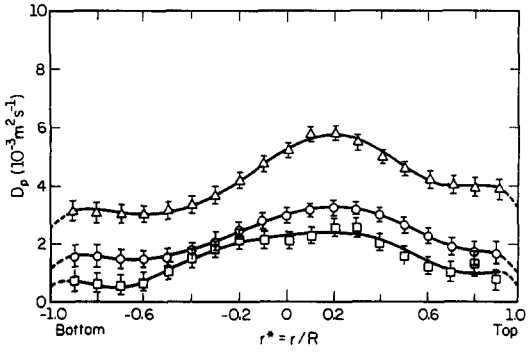

Figure 13. Influence of pipe Re on the particle diffusivity distribution along a vertical diameter. Key as in figure 9.

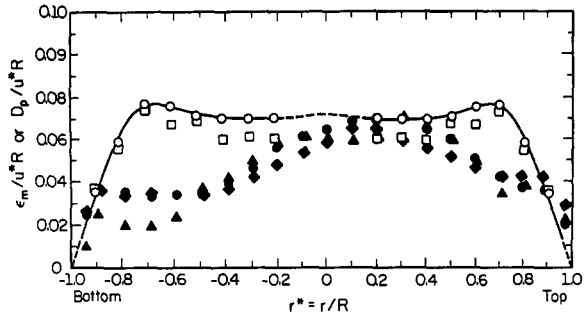

Figure 14. Generalized plot of the air and particle diffusivity distributions along a vertical diameter in horizontal, fully developed pipe flows of dilute suspensions.

Particle diffusivity		Air diffusivity		
W_0 (m/s)	Re		u^*/W_0	Re
▲ 10.6	7.21×10^4	○ Laufer's (1954) data	0.035	5×10^5
● 20.7	1.41×10^5	□ Nunner's (1956) data	0.045	3×10^4–6×10^4
◆ 31.6	2.15×10^5			

4.3. Electrostatic effects on particle diffusivity

All results presented in the previous two sections are for alumina particles that were naturally charged by contact. The relative humidity of the carrier air was high, $\geqslant 60\%$. The charge-to-mass ratio was low, being of the order of 10^{-6} C/kg. To investigate the effect of electric charge on the dynamics of suspension flows, and hence the particle diffusivity, the charge carried by the particles was increased 10–100 times by using a corona charger together with humidity control. Histograms of the charge spectrum and distributions of the mean q/m_p along a vertical diameter were obtained for all three Re, in addition to distributions of ρ_p and G. While the electric force varied directly with ρ_p, its effect was suppressed at high air velocities due to the dominating influence of turbulent diffusion. When $W_0 = 31.6$ m/s ($\mathrm{Re} = 2.15 \times 10^5$), a change in q/m_p from -7.6×10^{-7} to $+1.6 \times 10^{-4}$ C/kg had almost no effect on the particle axial velocities and only a minor influence on the inverse relaxation time and particle diffusivity. This indicates that, under the conditions of the present investigation, the particle velocity is primarily determined by the particle–fluid interactions. In the interest of conserving space, the readers are referred to the dissertation by Ni (1986) for details.

5. AN APPROXIMATE RELATION FOR PARTICLE DIFFUSIVITY

The experimental finding that at sufficiently large Re and Fr, both D_p and F are basically governed by fluid–particle interactions, with electrical and gravitational effects playing a secondary role, prompts us to seek a general representation for D_p in horizontal, fully developed, turbulent pipe flow of dilute suspensions.

For the Brownian diffusion of a small spherical particle of radius a in a quiescent, isothermal fluid, Einstein (1906) showed that $D_p = kT/6\pi\mu a$, where k is the Boltzmann constant and T is the absolute temperature of the fluid. Since the inverse relaxation time for a spherical particle in Stokes motion is $F_S = 9\mu/2a^2\bar{\rho}_p$, Einstein's result can be rewritten as $D_p F_S = kT/m_p$. Thus, for Brownian diffusion, $D_p F_S$ is a constant.

An examination of the pairs of figures for F and D_p (figures 7 and 8; figures 12 and 13) reveals that the distribution of F along a diameter of the cross section is almost the mirror image of the distribution of D_p along the same diameter. Thus, the temptation is great to see if their product is a constant. In figure 15(a), the product $D_p F$ is plotted vs r^* for $\phi = 0°$, 30°, 60° and 84°. While some scatter is evident, the conjecture that $D_p F = \text{const}$ over a cross section is indeed a valid approximation. Figure 15(b) shows the product $D_p F$ for three air velocities; it is seen that $D_p F$ at the centerline varies directly with Re. In other words, the ratios of $(D_p F)_0$ and the ratios of W_0 are closely identical; they are approx. 2.9 : 1.9 : 1. This finding is expected in view of the normalized particle diffusivity data shown in figure 14, and the fact that F is almost constant at

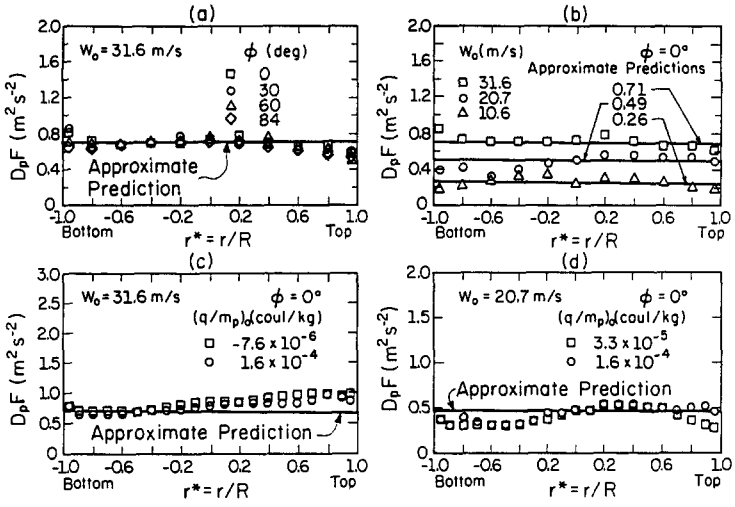

Figure 15. Comparison of the proposed approximation. $D_pF = \epsilon_{m0}(9\chi\mu/2a^2\bar{\rho}_p)$, with the measured data. In (a) and (b), $(q/m_p)_0 = 2.36 \times 10^{-6}$ C/kg.

the pipe centerline. For both figures 15(a) and (b), the particles are very weakly charged. Figure 15(c) shows the distributions of D_pF along a vertical diameter for two widely different particle charge-to-mass ratios at $W_0 = 31.6$ m/s. Similar data are plotted in figure 15(d) for $W_0 = 20.7$ m/s. Thus, for all cases examined, the following approximate relationship holds:

$$D_pF \cong C, \qquad [16]$$

where C is a constant over the pipe cross section. The deviation of C from being a constant increases as q/m_p increases and as Re or Fr decreases.

At the pipe centerline, the velocity lag between the fluid and the particle is small, and the particle diffusivity may be approximated by that of the fluid. Denoting all quantities at the pipe center by the subscript 0, we have $D_{p0}F_0 = C$ with $D_{p0} \simeq \epsilon_{m0}$ (ϵ_{m0} being the eddy diffusivity for momentum transfer for the fluid) and $F_0 = \chi C_0^* F_S$ (C_0^* being the correction for deviation from Stokes motion). When D_{p0} is taken to be ϵ_{m0}, it is overestimated, as shown in figure 14. If, on the other hand, we set $C_0^* = 1$, then $F_0 = \chi F_S = 9\chi\mu/2a^2\bar{\rho}_p$. F_0 evaluated in this manner would be underestimated. Due to the compensatory nature of the two error sources, the product (D_pF) may be approximated by $\epsilon_{m0}(9\chi\mu/2a^2\bar{\rho}_p)$—as shown by the solid lines in figures 15(a)–(d). Hence, we tentatively recommend

$$C \cong \epsilon_{m0}\left(\frac{9\chi\mu}{2a^2\bar{\rho}_p}\right). \qquad [17]$$

With $D_pF = C$, [4a] and [4b] can be integrated to give

$$\frac{\rho_p}{\rho_{p0}} = \exp\left[-C^{-1}\left(\int_0^r \frac{q}{m_p}\frac{\partial V_e}{\partial r}\,dr - gr\cos\phi\right)\right]. \qquad [18]$$

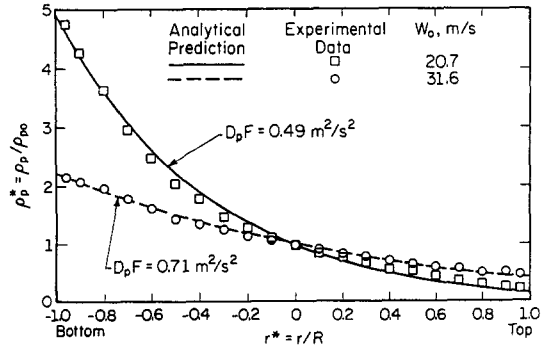

Figure 16. Comparison of the measured particle density distribution along a vertical diameter with predictions based on the D_pF = const model.

To assess the usefulness of the approximate relation for C, the experimentally measured ρ_p along a vertical diameter for $W_0 = 20.7$ and 31.6 m/s are compared in figure 16 with those calculated from [18] with $\phi = 0$ and with C evaluated from [17]. The comparison is very satisfactory. It should be noted that for the two cases shown in the figure, $(q/m_p)_0 = 1.20 \times 10^{-6}$ and 7.62×10^{-6} C/kg, respectively for $W_0 = 20.7$ and 31.6 m/s, and hence the electric effect is small.

6. CONCLUSIONS AND CONCLUDING REMARKS

Under conditions within the limits of the present investigation, the turbulent diffusivity of small particles in a steady, fully developed, turbulent flow of dilute suspensions in a horizontal, electrically grounded conducting pipe is governed essentially by the fluid–particle interactions. At sufficiently high pipe Re and large Fr, the gravitational and electrical forces have only a very minor influence on the particle diffusivity. The approximate phenomenological relation $D_p F = C$, with $C \simeq \epsilon_{m0}(9\chi\mu/2a^2\bar{\rho}_p)$ can be used to estimate the particle diffusivity distribution over the pipe cross section. Future research should be directed to establish the limits of validity of the proposed relation by extending the ranges of the pipe Re, Fr, particle size, particle phase density and charge-to-mass ratio. Comparison of the diffusivity data with those evaluated directly from the particles' instantaneous velocities measured by LDV is highly desirable.

Acknowledgement—The authors wish to express their appreciation for the support of this work by the National Science Foundation under Grants NSF CPE 8317615 and 8405866.

REFERENCES

CHAO, B. T. 1964 Turbulent transport behavior of small particles in dilute suspension. *Öst. Ing. Arch.* **18,** 7–21.

CHAO, B. T. 1981 Scaling and modeling. In *Handbook of Multiphase Systems*, Chap. 3 (Edited by HETSRONI, G.), pp 3-44–3-49. Hemisphere/McGraw-Hill, Washington, D.C. /New York.

CHENG, L., TUNG, S. K. & SOO, S. L. 1970 Electrical measurements of flow rate of pulverized coal suspension. *Trans. ASME Jl Engng Power* **92,** 135–149.

CSANADY, G. T. 1963 Turbulent diffusion of heavy particles in the atomsphere. *J. atmos. Sci.* **20,** 201–208.

EINSTEIN, A. 1906 Zur Theorie der Brownschen Bewegung. *Annln. Phys.* **19,** 371–381.

HINDS, W. C. 1982 *Aerosol Technology*. Wiley, New York.

HINZE, J. O. 1975 *Turbulence*. McGraw-Hill, New York.

LAUFER, J. 1954 The structure of turbulence in fully developed pipe flow. Report NACA TN-1174.

LUMLEY, J. L. 1957 Some problems connected with the motion of small particles in turbulent fluid. Ph.D. Thesis, The John Hopkins Univ., Baltimore, Md.

MEEK, C. C. & JONES, B. G. 1973 Studies of behavior of heavy particles in a turbulent fluid flow. *J. atmos. Sci.* **30,** 239–244.

NI, S. 1986 Particle diffusivity in fully developed turbulent pipe flow of dilute suspensions. Ph.D. Thesis, Univ. of Illinois, Urbana-Champaign, Ill.

NIEH, S., CHAO, B. T. & SOO, S. L. 1985a Interaction of gravity and electrostatic effects in pipe flow of a gas–particle suspension. *Particulate Sci. Technol.* **3,** 127–148.

NIEH, S., CHAO, B. T. & SOO, S. L. 1985b Effect of electrostatic charge distribution on the dynamics of a solid particle in a gaseous suspension. *J. Pipelines* **5,** 137–145.

NIEH, S., CHAO, B. T. & SOO, S. L. 1986 An electrostatic induction probe for measuring particle velocity in suspension flow. *Particulate Sci. Technol.* **4,** 113–130.

NUNNER, W. 1956 Warmeüergang und Druckabfall in Rauchen Rohren. *VDI Forsch Hft* **455.**

SOO, S. L. 1956 Statistical properties of momentum transfer in two-phase flow. *Chem. Engng Sci.* **5,** 57–67.

SOO, S. L. 1973 Flow of suspensions, In *Von Karman Inst. Fluid Dynam. Lect. Ser. No. 21, Fluid Dynamics of Particulate Systems*. Rhode-Saint-Genese, Belgium.

SOO, S. L. 1978 Diffusivity of spherical particles in dilute suspensions. *AIChE Symp. Ser.*, No. 174. *Heat Transfer* **74,** 184–185.

Soo, S. L. 1983 *Multiphase Fluid Dynamics*, preliminary revised edn. S. L. Associates, Urbana, Ill.

Soo, S. L., Trezek, G. J., Dimik, R. C. & Hohnstreiter, G. F. 1964 Concentration and mass flow distributions in a gas solid suspension. *Ind. Engng Chem. Fundam.* **3,** 98–106.

Soo, S. L., Stukel, J. J. & Hughes, J. M. 1969 Measurement of mass flow and density of aerosols in transport. *Envir. Sci. Technol.* **13,** 386–393.

Tchen, C. M. 1947 *Mean Value and Correlation Problems Connected with Motion of Small Particles Suspended in a Turbulent Fluid.* Nijhoff, The Hague, The Netherlands.

Tsuji, Y. & Morikawa, Y. 1982 LDV measurements of an air–solid two-phase flow in a horizontal pipe. *J. Fluid Mech.* **120,** 395–409.

Turner, G. A. & Blasubramanian, M. 1976 The frequency distributions of electrical charges on glass beads. *J. Electrostat.* **2,** 85–89.